Journal of Aerosol Science 170 (2023) 106158

Contents lists available at ScienceDirect

Journal of Aerosol Science

journal homepage: www.elsevier.com/locate/jaerosci

Singularly narrow size distributions of 200 nm polystyrene latex spheres determined by high resolution mobility analysis

Juan Fernandez de la Mora [a,*], John Kramar [b], Natalia Farkas [b,c], Steven Papanu [d], Robert Dana [e]

[a] Yale University, Department of Mechanical Engineering and and Materials Science, New Haven, CT, 06511-8286, USA
[b] National Institute of Standards and Technology, Gaithersburg, MD, 20899, USA
[c] Building and Fire Sciences, US Forest Service, Forest Products Laboratory, 1 Gifford Pinchot Drive, Madison, WI, 53726, USA
[d] 2520 Wyandotte Street Suite F, Mountain View, CA, 4083-2381, USA
[e] NanoEngineering Corporation, 1204 Main Street, #262, Branford, CT 06405, USA

ARTICLE INFO

Handling Editor: Chris Hogan

Keywords:
Polystyrene
Spheres
Size standard
Narrow size distribution
Aerosol
Gas phase
Bipolar electrospray

ABSTRACT

A high-resolution differential mobility analyzer (DMA) is used for the first time to study the mobility distribution of Polystyrene Latex (PSL) particles. We investigate in particular some unique, nominally 200 nm and 100 nm PSL particles, known by other methods to be unusually monodisperse. The suspensions are electrosprayed after adding ammonium acetate to a concentration of 10 mmol/L. Mobility analysis is carried out after charge reduction with a second electrospray of the opposite polarity. The 200 nm particles typically produce two narrow peaks, with relative intensities that depend on electrospray parameters. Under the most favorable spraying conditions achieved, the more mobile peak becomes dominant, is narrowest, and has a repeatable mobility; we attribute it provisionally to the unpolluted suspended particles. The less mobile peaks are substantially more variable but never entirely removed. We initially attributed them to attachment of involatile solutes in the suspension to the atomized PSL particles; however, this hypothesis is put in doubt by later observations. The measured relative width of the mobility distribution for the most mobile peak is $FWHM_Z = (1.65 \pm 0.08)$ %. This translates into a width for the diameter distribution $FWHM_d = (1.09 \pm 0.05)$ % or standard deviation $\sigma_d = (0.46 \pm 0.02)$ %, by far the most monodisperse polymeric submicron particle suspension so far reported. Concentrations of ammonium acetate of 100 mmol/L and 40 mmol/L were also tested in order to reduce residue attachment by forming smaller initial electrosprayed drops. These higher salinities, however, led to capillary clogging, apparently because the narrow electrospraying jet precludes the passage of the PSL particles. The 100 nm particles gave a wider variation in mean diameter and size distribution depending on electrospraying parameters, perhaps because of the suspension's considerably larger content of involatile solutes. Unlike the 200 nm particles, no spraying condition was found under which a precisely repeatable size distribution could be achieved for the 100 nm particles. However, the data do point to an estimated upper bound on the size distribution width of $FWHM_d \approx 3$ % ($\sigma_d \approx 1.3$ %), which is uniquely narrow for particles of this size.

* Corresponding author.
E-mail addresses: juan.delamora@yale.edu (J. Fernandez de la Mora), pearlglo@comcast.net (S. Papanu).

https://doi.org/10.1016/j.jaerosci.2023.106158
Received 11 December 2022; Received in revised form 15 February 2023; Accepted 16 February 2023
Available online 22 February 2023

1. Introduction

Size standards are widely used in many fields, for metrology, sizing instrument calibration. etc. Applications include micro-contamination measurement in semiconductor processing, atmospheric sampling, and electron-microscope calibration. Polystyrene Latex (PSL or "latex") spheres have been widely used as size standards, due to a number of advantages such as the longevity of their suspensions and the ability to produce them in relatively narrow size distributions. For instance, the particle technology catalog of Thermo Scientific offers a series of NIST-traceable polystyrene latex (PSL) particles[1] with diameters d ranging from 50 nm to 3 μm. The narrowest relative diameter distribution for this series occurs at a mean diameter of ≈800 nm, which is stated to have a relative full width at half maximum $FWHM_d$ of ≈1.8 % (relative standard deviation $\sigma_d \approx 0.8$ %). However, the narrowness of the distribution deteriorates markedly with decreasing size, with the ≈200 nm particles having a $FWHM_d$ of ≈4.0 % ($\sigma_d \approx 1.8$ %), the ≈100 nm particles having a $FWHM_d$ of ≈5.2 % ($\sigma_d \approx 2.6$ %), and the ≈50 nm particles having a $FWHM_d$ of ≈17 % ($\sigma_d \approx 7.5$ %). NIST's own SRM 1691 particles have been studied by several groups, all reporting a σ_d almost as narrow as 1 % ($FWHM_d = 2.35$ %) for particles of mean diameter 269 nm (Thomas et al., 1988). These distribution widths all relate to the diameter rather than the mobility distribution. For the mentioned metrology and calibration applications and many others, the availability of considerably narrower size distributions would be of great interest. The authors have recently investigated particles of non-enveloped viral species in the gas phase with high resolution mobility measurements, observing size distributions with $FWHM_d$ values below 1 % at mean diameters under 50 nm (Fernandez de la Mora et al., 2020, 2022). In fact, given the lack of standard particles of sufficient monodispersity, it has not yet been possible to separate the native distributions of the viruses, *vs.* the broadening effect from the finite resolving power of the mobility analyzers used. Below 100 nm, viral size standards appear to have narrower size distributions than PSL particles. On the other hand, viral standards present other problems. They may be stable only in suitable buffer solutions characterized by high concentrations of involatile electrolytes. They become unstable with modest changes in temperature and pH, or upon exchanging the original viral buffer for one containing the volatile salts required for cleanly electrospraying the virus into the gas phase. Thus, PSL standards would be more practical than viral standards if they were available with comparably narrow size distributions.

In the present study we combine recent developments in the synthesis of PSL suspensions with advances in mobility instrumentation allowing high-resolution measurements of singularly narrow distributions with $FWHM_Z$ values as small as 1 % in electrical mobility. Based on the Millikan relation between mobility and diameter in ambient air, the corresponding $FWHM_d$ in diameter is about half that value for particles smaller than 60 nm. These combined tools have allowed us to demonstrate that such narrow PSL size distributions do in fact already exist. Our study follows a long tradition of prior investigations involving mobility measurements of PSL particles (Kim et al., 2005; Kinney et al., 1991; Mulholland & Bauer, 2000; 2006; Myojo et al., 2004). Note finally that $FWHM$ and σ reported in this work are not the true values for the measured distribution, but those pertaining to a Gaussian distribution obtained as best fit to the data.

2. Experimental

PSL particles of nominal size 100 nm and 200 nm were synthesized by one of us (S·P.) using a proprietary process, and are available to other potential users. These particles are being investigated at NIST for their possible use as size standards. The 100 nm latex contained ≈0.64 % latex solids by mass and ≈0.15 % non-polymer solids, either attached to the particles or dissolved in the water. The 200 nm latex was produced by a substantially different formulation and contained ≈0.99 % latex solids and only ≈0.008 % non-polymer solids by mass. A special preparation of the 200 nm particles free from involatile solutes was also measured.

The particles were electrosprayed (ES) in positive polarity, near their original concentration, with the minimal dilution required by the addition of ammonium acetate (AA). In a few tests, the 100 nm particles were diluted in deionized water by factors of either 5 or 10. In most cases for which data are reported here, the sprayed solutions incorporated 10 mmol/L to 12 mmol/L ammonium acetate (AA), since the volume of ES drops is approximately inversely proportional to the electrical conductivity of the solution (Fernandez de la Mora & Loscertales, 1994). To achieve this concentration, a small volume of a 0.5 mol/L aqueous solution of AA was added to the PSL dispersions. As electrosprayed, these large particles hold an excessive number z of elementary charges for unambiguous inference of their size based on a mobility measurement alone. Accordingly, the high original particle charge states (z of hundreds) were drastically reduced by opposing to the positive capillary a negative capillary producing small anions, an arrangement referred to as a bipolar ES. A grounded metallic grid placed symmetrically between both emitters decoupled them electrostatically, facilitating stable bipolar emission (Fernandez de la Mora & Barrios, 2017). Two variants of the negative emitter were used. In one, the sprayed liquid was deionized water. In this case there was no genuine negative electrospray with a conical meniscus, but a mild electrical discharge from a smooth convex liquid tip. The emission currents could be unusually small, even below 10 nA, which is helpful to produce positive PSL charge states in excess of $z = 15$ (Fig. 1). In the second negative emission scheme, the spraying liquid was methanol with 10 mmol/L AA, and the meniscus was conical. Both approaches produced comparable results, except that the smallest negative current that could be stabilized from the 10 mmol/L AA methanol solution was of the order of 100 nA. Suspensions with 10 mmol/L AA remained stable for at least several weeks, as indicated by the steady quality of the mobility spectra obtained. A few experiments with considerably smaller or larger electrolyte content (from de-ionized water to 100 mmol/L AA) will also be reported.

[1] Certain commercial equipment, instruments, and materials are identified in this paper to foster understanding. Such identification does not imply recommendation or endorsement by the National Institute of Standards and Technology, nor does it imply that the materials or equipment identified are necessarily the best available for the purpose.

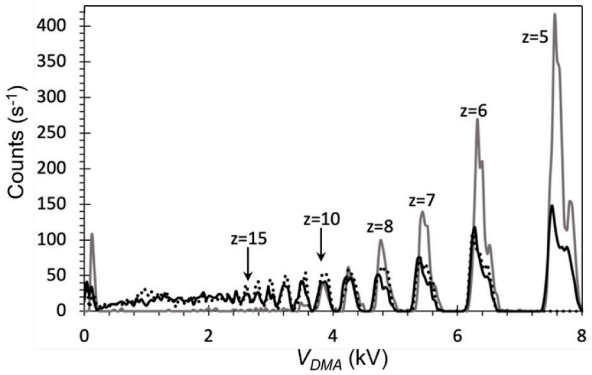

Fig. 1. Triplicate mobility spectra of 200 nm PSL particles taken under nominally identical conditions, exhibiting multiple peaks associated with different charge states, $z = 5, 6, 7, \ldots$, from right to left. Note the bimodal and perhaps also trimodal peaks in the better resolved right side of the figure.

The flow rate q of air through the bipolar ES chamber was in the range from 0.15 L/min to 0.4 L/min. It was all sent to the polydisperse aerosol inlet of the DMA, and coincided also with the flow rate of size-selected aerosol at the DMA outlet.

The mobility measurement was carried out with a differential mobility analyzer (DMA). This instrument combines a radial electric field with a flow field of clean air moving axially at a large flow rate Q between two coaxial cylindrical electrodes (Knutson & Whitby, 1975). The electric field is created by establishing a voltage difference V between the two electrodes. Ions carried at a small sample flow rate q of air entering inwards through a narrow slit in the outer electrode are dispersed by the electric field in fan-like trajectories, such that only the ions within a narrow range of electrical mobilities Z exit through a second narrow slit in the inner electrode, and are sampled into a detector. When operating the DMA with a recirculating sheath flow ensuring that the sample flow rate q is the same at both slits, the selected mobility Z is such that the ratio

$$k=VZ/Q \tag{1}$$

is a constant that depends only on the DMA geometry. For cylindrical electrodes, this constant has a known dependence on the radii of the two electrodes and the axial distance between the two slits (Knutson & Whitby, 1975). Our inner electrodes are not perfectly cylindrical but rather slightly conical to delay turbulent transition, hence k must be determined empirically by calibration. A mobility spectrum is obtained by scanning over the voltage difference V at fixed flow rates q and Q and recording the signal (counts per second) of classified particles detected as a function of V (Fig. 1). The uncertainty in the voltage measurements is negligible, about 0.1 % digitization scale error. The detector was an experimental variant of a commercial condensation particle counter (CPC). It condenses water vapor on the PSL particles, growing them into sizes large enough to be individually counted optically.

Flow rates Q were measured with a commercial mass flow meter covering up to 220 L/min. The instrument determines mass flow rate and reports it as standard volumetric flow rate at 20 °C and 101.3 kPa. The manufacturer specifies a maximal error of ±2 % in the measured flow rate, with reproducibility of ±0.75 %.

The DMA used primarily in this work (denoted Perez-MT) is a variant of another recently described (the Perez-LT DMA of Perez-Lorenzo & Fernandez de la Mora, 2021) where the geometry of the inner electrode is widened to reduce its separation from the outer electrode. This results in a smaller value of the constant k, which favors the classification of the relatively large particles presently investigated. k has units of an inverse length, but will be quantified here with the more practical units $(cm^2{\cdot}s^{-1})/(L/min)$. The new value $k_{MT} = (0.0582 \pm 0.001)$ $(cm^2{\cdot}s^{-1})/(L/min)$ was determined by comparing mobility spectra for the 200 nm PSL particles obtained with the MT and the LT DMAs (Fig. SI–1). The ±2 % ambiguity assigned to this measurement is discussed in the Supplementary Information. All the estimated uncertainties presented are one standard deviation, and only include type A statistical contributions (JCGM, 2008), except where otherwise stated.

Fig. SI–1 has the additional general interest of demonstrating that the present 200 nm PSL particles already constitute a reliable reference material, even though its precise diameter has not yet been determined.

Note that singly charged 200 nm particles in ambient air have a fairly low electrical mobility $Z_1 = 0.087\ cm^2{\cdot}kV^{-1}{\cdot}s^{-1}$. Accordingly, their classification at the largest voltage difference $V = 9.0$ kV sustained by the MT-DMA requires the use of a relatively small flow rate $Q < 13$ L/min. Since DMA resolving power $FWHM_Z$ is limited by the ratio Q/q (Knutson & Whitby, 1975), to analyze these particles at a resolution of 100 requires a rather small sample flow rate $q < 0.13$ L/min. Because this results in inconveniently small detected signals, we used flow rates Q and q substantially larger than 13 L/min and 0.13 L/min to classify particles with five to fifteen positive charges after ES ionization and bipolar charge neutralization. For the moderate charge levels z used in this work, the mobility of these particles is approximately proportional to z:

$$Z(z) \approx zZ_1, \tag{2}$$

where Z_1 is the mobility of the singly charged particles. Therefore, when reporting the mobilities of multiply charged particles, we will give the quantity $Z_1 = Z(z)/z$ common to all charge states. We should note there is a slight but measurable increase with z of the ratio

$Z(z)/z$. This "drag reducing" effect of the charge is of some theoretical interest, as the known trend for small particles in the free molecule-regime is the opposite (Tammet, 1995; Fernández-García & Fernándezde la Mora, 2013, 2014).

3. Results for 200 nm particles

3.1. Bimodal size distributions from 10 mmol/L AA solutions

The mobility spectra obtained with this sample are exceptionally clean: With the exception of a high mobility peak (probably produced by residues from dried spray drops not containing any PSL particle), hardly any spectral feature is seen other than the peaks corresponding to the various charge states z of the PSL particles. Fig. 1 shows three mobility spectra, each obtained with $Q = 53$ L/min and $q = 0.26$ L/min. The right-most peak corresponds to particles with 5 charges (z = 5), the one to its immediate left to z = 6, etc., with recognizable peaks beyond $z = 15$. One can hardly see any background signal between the peaks corresponding to the lowest charge states ($z = 5, 6, 7, \ldots$). An unexpected feature is that the best resolved peaks are clearly bimodal, with occasional indications of a third mode. We have not previously observed this peak duplication in suspensions of viruses having a unique structure, where we always remove small non-volatile solutes by dialysis. The fact that the PSL suspensions had not been dialyzed suggested initially that the secondary peaks corresponding to the larger particles were due to a crust of involatile suspension solutes deposited on the PSL spheres upon drying of the atomized drops. Indeed, conventional wisdom in electrospraying small particles and large molecules has dictated the need to remove all involatile solutes, while introducing relatively high concentrations (≈100 mmol/L) of involatile salts to minimize the initial electrosprayed drop volume (and hence the total mass of involatile residue). However, the situation here is different because the PSL particles are larger than typical ES drops. Notice in the far left of Fig. 1 the presence of a peak, at a mobility of about 28 $cm^2 \cdot kV^{-1} \cdot s^{-1}$, corresponding to a diameter of ≈8.6 nm. An indication of the fraction of all involatile solutes in the suspension may be obtained by assuming that the relatively mobile particles observed result from the drying of initial ES drops containing just involatile solutes with no PSL spheres. Kaufman et al. (1996) have previously investigated these pure residues. They estimate an initial drop diameter of 100 nm for a 20 mmol/L AA solution. Given the inverse relation between sprayed drop volume and ion concentration (Fernandez de la Mora & Loscertales, 1994), our initial ES drops would have an initial diameter of ≈130 nm. The volume fraction of involatile solutes in this suspension may then be rather roughly estimated as $\approx(8.6\ \text{nm}/130\ \text{nm})^3 = 0.029$ %. This is almost four times above the 0.008 % solids directly measured for this suspension, suggesting that a mechanism producing anomalously large initial drops is acting here. An anonymous referee has noted that the calculated ES drop diameter of ≈130 nm is smaller than the 200 nm PSL spheres. Furthermore, these drops are released by the breakup of a jet produced at the tip of the Taylor cone, whose diameter is typically about 1.8 times smaller than the drop diameter. This means that the 200 nm PSL particles must go through a jet which, absent the PSL, would have a diameter of about 130 nm/1.8 ≈ 70 nm! It is accordingly possible that the bimodal size distributions found could result from an anomalous jet breakup mechanism due to the presence of such large particles. This possibility has led us to various attempts to eliminate the bimodal distributions by modifying the composition of the suspension containing the particles.

3.2. Results from high conductivity solutions

The suspicion of a serious effect of the mismatch between the usual diameter of the ES jet and the PSL spheres was strongly confirmed by experiments with suspensions incorporating 40 mmol/L and 100 mmol/L AA. These resulted in quick clogging of the capillaries, which we first attributed to flocculation. However, this interpretation proved incorrect because, before clogging, we were able to obtain clean mobility spectra without any peaks associated with dimers or trimers. Clogging was in fact due to accumulation of PSL in the Taylor cone as a result of the inability of the particles to be carried by the considerably smaller jets formed by these conducting solutions. This behavior was particularly clear from the fact that a Taylor cone would remain after the flow of liquid was substantially blocked. Evidently, the Taylor cone was mostly of PSL that had accumulated and filled the original liquid meniscus. The

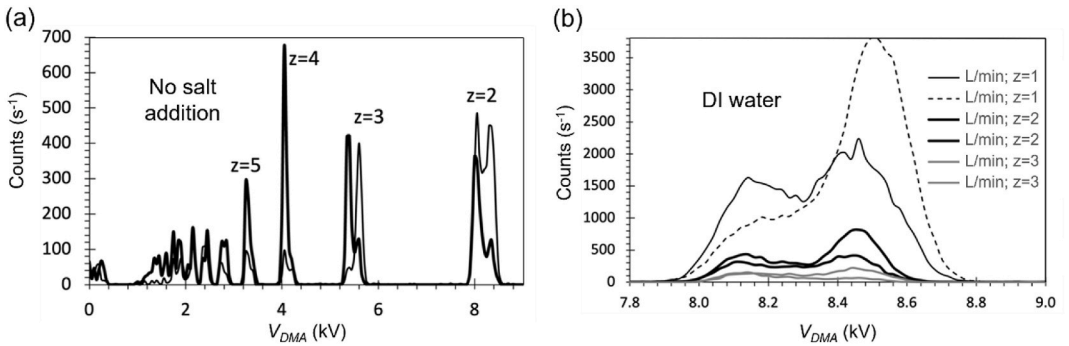

Fig. 2. Mobility spectra of 200 nm PSL particles in buffers of decreasing conductivity, resulting in ES jets with diameters definitely larger than the PSL particles. The bimodal structure is nevertheless preserved. (a) Original suspension without addition of AA. (b) Suspension free from volatile and involatile solutes.

clogging was undoubtedly of a combustible material, as it quickly cleared out when sucking air from the room into the capillary tip in the presence of a flame. The clear conclusion from these tests is that there is a limit to the allowable mismatch between the natural ES jet diameter and the particle diameter. Beyond this limit, rather than being atomized, the particles are trapped in the meniscus and block the capillary.

3.3. Tests with low conductivity solutions

While 10 mmol/L AA solutions do not block the passage of 200 nm PSL particles, it is conceivable that partial blocking would arise, resulting in unsteady atomization. Perhaps, successive blocking and unblocking events would produce a succession of large and small drops, responsible for the observed bimodal atomization pattern. This imaginary scenario suggested the interest of electrospraying from considerably less conducting solutions.

In a first attempt, we simply sprayed the original PSL suspension without any addition of volatile electrolyte. This still produced a bimodal size distribution (Fig. 2a).

Next, we used the pure aqueous suspension of the same 200 nm PSL particles, that contained no solutes other than the PSL particles. The corresponding ES jet was evidently much wider than for the 10 mmol/L AA solution, as it could be clearly seen in the optical microscope used to monitor the Taylor cone. Still, the mobility distributions were bimodal and comparable to those observed in 10 mmol/L AA solutions (Fig. 2b).

In view of the new availability of PSL suspensions free from involatile solutes, we proceeded to spray them with an ionic concentration similar to that in 10 mmol/L AA. To avoid possible bacterial growth, we replaced the AA with 2.2 % formic acid, whose known dissociation constant yields a predicted ion concentration of 10 mmol/L. Surprisingly, these *conducting pure aqueous* suspensions produced mobility spectra with bimodal structures very similar to those from the original 200 nm PSL suspension.

The conclusion from these various tests is that the origin of the double peaks in the 200 nm particles is neither contamination from involatile solutes accompanying the suspension, nor the possible interference in the atomization process from suspended particles larger than the jet diameter. Also, it is difficult to envision how the low mobility peak could be part of the size distribution of the PSL, since the relative magnitude of the two peaks observed varies widely depending on the spraying conditions (Figs. 1 and 2). Preliminary scanning electron microscopy (SEM) measurements of these nanoparticles deposited on Si substrates reveals a size distribution slightly wider than the mobility measurement, with no evidence of a bimodal distribution. The hypothesis that SEM misses a putative double peak due to insufficient resolution can be rejected because the combined widths of the two DMA peaks exceed amply the SEM width. The second DMA peak is accordingly an artifact of the atomization process. Whatever its origin, we have been unable to remove entirely the low mobility peak and will have to live with it for the time being. This situation complicates the use of these particles as reference materials for aerosol applications, since there is a risk of confusing one of the reference peaks with the other. Nevertheless, Fig. SI–1 included in the Supplementary Information shows that the two narrow mobility peaks produced by this material can certainly be used to obtain an accurate relative calibration of aerosol instruments.

3.4. Charge distribution

Fig. 3a illustrates the approximate validity of the linear relation (2) between mobility and charge state by representing several additional mobility spectra at various Q values, using the ratio Z/Z_1 as horizontal coordinate. Although the spectra shown do not include the singly charged ion, there is no ambiguity in the charge state based on other spectra (not shown) that did capture the $z = 1$ ion at lower Q values. All the peaks fall rather close to an integer number. The better resolved peaks on the left side of the figure show the bimodal mobility distribution already discussed. Naturally only one of these two peaks may fall at an integer value for any single choice of Z_1. Interestingly, in the range $5 < z < 13$, where the two modes are well resolved from each other, the lower mobility peak is dominant at low charge states, while its magnitude weakens and virtually disappears as z approaches 13. High charge states are

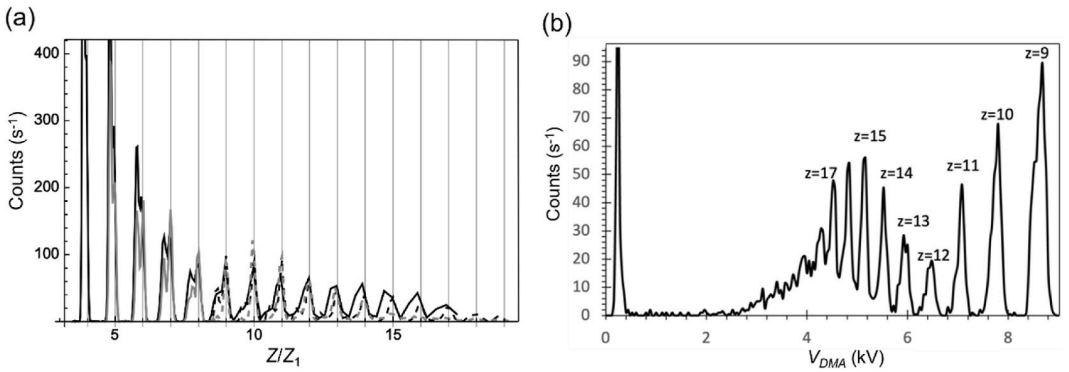

Fig. 3. Several spectra of 200 nm PSL particles. (a) CPC signal versus Z/Z_1: The peaks fall over integer numbers confirming the linear relation (2), $Z(z)=z\,Z_1$. Note that the low mobility peak dominating at low charge states decays quickly with z and has almost vanished at $z = 13$. (b) CPC signal versus V_{DMA}, illustrating the existence of a bimodal charge distribution.

accordingly less affected by our mysterious peak duplicating mechanism. Fig. 3b shows another interesting peculiarity of high charge states, through a clear instance where the charge distribution is bimodal. The height of the peaks exhibits two maxima: One centered at $z = 2$ or 3 (as observed in spectra not shown, obtained at lower Q and capturing lower z values), and another typically above $z = 10$ ($z = 15$ in Fig. 3b). A high z peak intensity mode is also identifiable in some of the spectra in Fig. 3a. The observation of two modes for both the size and the charge begs the question of a possible single mechanism responsible for both. Ordinarily spray drops having smaller initial volumes would carry fewer involatile solids, while the final charge would be controlled through the Rayleigh limit (Rayleigh, 1945) by the final drop size (the PSL diameter), irrespective of the initial drop size. This generally accepted scenario certainly does not fit our observations. However, the shrinking of the initial drops is controlled not only by water evaporation at fixed charge, but also by a sequence of Coulombic explosions providing a discontinuous means to reduce the charge with little ejection of liquid volume. The peculiarity arising in the presence of surfactants is that Coulombic explosions remove very effectively the surface material, which would increase the surface tension of the drop, increasing also the maximal charge it could carry at its fixed final size of 200 nm (Rayleigh's limiting charge). This would provide a plausible mechanism for the lesser contamination level observed in the highest charge states found. In contrast to Fig. 3a, some of the lowest z peaks in Fig. 3b seem to exhibit at least two modes, apparently dominated by the one with the lowest mobility. Nevertheless, the various modes presumably present in Fig. 3b are not sufficiently well resolved to enable drawing conclusions firm enough to contradict those inferred from the much better resolved peaks of Fig. 3a.

The apparently random variability in the relative height of these twin peaks may be better appreciated in Fig. 4. These measurements zoom in on the DMA voltage range from 8 kV to 9 kV, to better characterize actual peak shapes via a smaller stepping voltage in the mobility scan. Fig. 4 represents the CPC signal as a function of the electrical mobility $Z_1 = kQ/(Vz)$, at a fixed aerosol flow rate $q =$ 0.22 L/min and variable sheath gas flow rate Q. At $Q \approx Q_o = 11.6$ L/min, singly charged particles appear in the 8 kV–9 kV voltage interval. Therefore, given that the classification voltage V obeys $k = zVZ_1/Q$, particles carrying z elementary charges appear within the same voltage interval when the flow rate Q of sheath gas takes a value close to zQ_o. The increasingly narrow peaks that are seen in Fig. 4 correspond to increasing charge states and flow rates Q, collected in Table 1. Notice that the most mobile peak maintains a fairly fixed position at a mean value of (0.0816 ± 0.0003) cm^2·kV^{-1}·s^{-1}, corresponding to a mean diameter of $(209.2 \pm 0.7$ nm). In contrast, the features to its left shift position slightly from one experiment to the other, and, in some instances, decrease substantially in height.

Fig. 5 collects the relative widths $FWHM_Z$ inferred from the spectra of Fig. 4 for the most mobile peak in each pair. Rather than ignoring the low mobility feature, we have fitted the full spectra to a linear combination of three Gaussians with optimally selected independent means, and the same standard deviation (to facilitate convergence). The reliability of this procedure is confirmed by the fact that it provides an excellent fit to the high mobility part of the main peak. One sees that the high charge states (smaller q/Q) cluster with some variation around a relatively small width, which we interpret as intrinsic to the particles. The figure shows the squares of the width and of q/Q, to facilitate separating known contributions to width from the DMA from those intrinsic to the 200 nm PSL sample, $FWHM_{Z\infty}$. The former is given as q/Q in the analysis of Knutson and Whitby (1975), which ignores diffusion (an excellent assumption for 200 nm particles selected at 8 kV). Since both contributions are independent, it is reasonable to follow earlier studies (Perez-Lorenzo et al., 2020 and references therein) in assuming an approximate quadratic additive rule:

$$FWHM_Z^2 = q^2/Q^2 + FWHM_{Z\infty}^2. \tag{3}$$

This is a convenient interpolation between the Knutson-Whitby limit $FWHM_Z = q/Q$ for a hypothetical monodisperse non-diffusive particle, and the opposite limit $FWHM = FWHM_{Z\infty}$ for a particle with a mobility distribution of finite width $FWHM_{Z\infty}$, classified in a hypothetical instrument of infinite resolving power. $FWHM_{Z\infty}^2$ may then be inferred by the intersection of the linear regression line with the y axis, yielding $FWHM_{Z\infty} = 0.000272^{1/2} = 1.65$ %. The uncertainty is estimated as the standard deviation of the individual $FWHM_Z$ values relative to the fit curve $FWHM_Z = [m\,(q^2/Q^2) + FWHM_{Z\infty}^2]^{1/2}$, 0.08 %. This statistical uncertainty in $FWHM_{Z\infty}$ is the dominant uncertainty component. The slope m of the linear fit would be expected to be unity but is in reality 1.624. A probable reason for the discrepancy is a possible error by a factor of 0.78 in the measurement of q. This is not unlikely, as the reference ball flowmeter

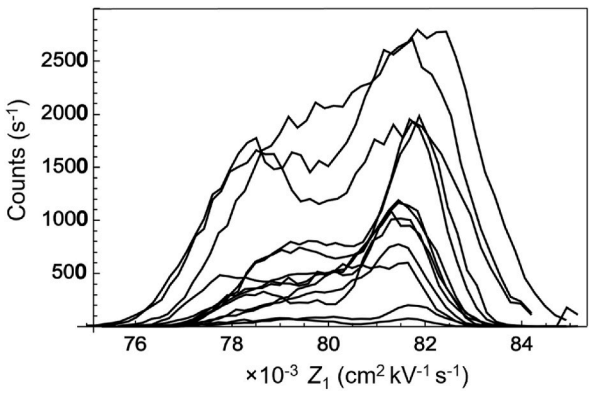

Fig. 4. Various mobility spectra of the nominally 200 nm PSL particles obtained at a fixed aerosol flow rate $q = 0.22$ L/min, and variable sheath gas flow rates and charge states. Decreasing widths and peak heights correspond to increasing z. By Millikan's relation, 200 nm particles would have a mobility of 87×10^{-3} cm^2·kV^{-1}·s^{-1}.

Table 1
Sheath gas flow rates Q, charge states z, mean V_{DMA} for main peaks, inverse relative full peak width $1/FWHM_Z$, electrical mobility Z_1 and flow rate ratios (q/Q) for the spectra of Fig. 4. The mean mobility is Z_{1avg}= (0.0816 ± 0.0003) $cm^2 \cdot kV^{-1} \cdot s^{-1}$, and the mean diameter is d_{avg} = (209.2 ± 0.7) nm. As discussed in the text, these modest statistical uncertainty estimates ignore the ±2 % calibration ambiguity discussed in the Supplementary Information.

Q (L/min)	z	V_{DMA} (kV)	$FWHM_Z^{-1}$	Z_1 ($cm^2 \cdot kV^{-1} \cdot s^{-1}$)	q/Q
11.7	1	8.284	35.2	0.0822	0.0188
11.6	1	8.265	34.3	0.0817	0.0190
11.6	1	8.259	33.1	0.0817	0.0190
23.3	2	8.332	49.6	0.0814	0.0094
23.3	2	8.325	50.7	0.0814	0.0094
23.3	2	8.367	49.7	0.0810	0.0094
35.2	3	8.353	57.5	0.0818	0.0063
35.2	3	8.343	53.2	0.0818	0.0063
46.8	4	8.357	53.3	0.0815	0.0047
46.8	4	8.350	53.6	0.0816	0.0047
58.5	5	8.363	57.3	0.0814	0.0038
58.5	5	8.365	57.4	0.0814	0.0038
81.7	7	8.311	65.1	0.0817	0.0027

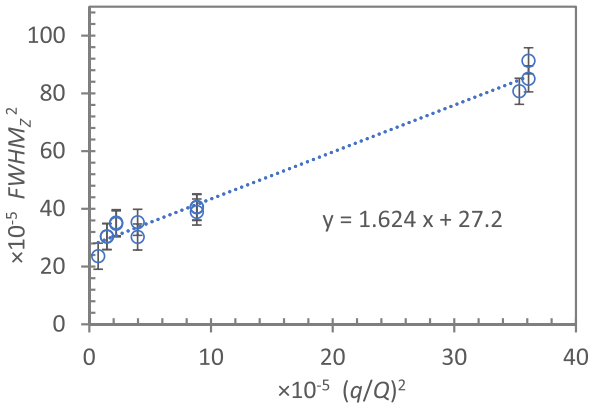

Fig. 5. Representation of the $FWHM_Z$ data from Table 1 in the form suggested by Equation (3). The zero intercept of the linear regression line yields the mean intrinsic width of the
mobility distribution, $FWHM_{Z\infty}$, and the standard deviation of the $FWHM_Z$ data relative to the fit curve $FWHM_{Zfit} = (m\ (q/Q)^2 + FWHM_{Z\infty}^2)^{1/2}$ provides an uncertainty estimate, yielding $FWHM_{Z\infty}$= (1.65 ± 0.08) %.

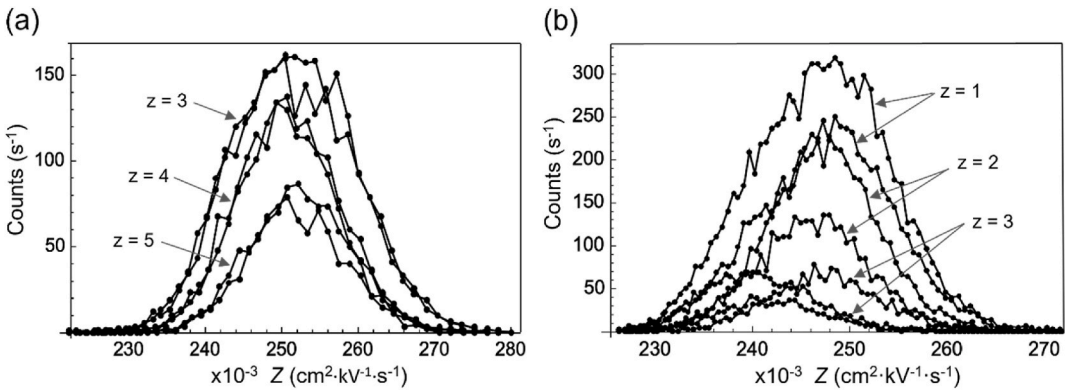

Fig. 6. Mobility spectra obtained with the 100 nm PSL particles at various flow rates and charge states z. (a) Data taken with the Perez-LT-DMA providing a mean mobility Z = 0.251 $cm^2 \cdot kV^{-1} \cdot s^{-1}$ for these particles. (b) Data obtained with the Perez-MT-DMA showing a mean mobility of Z = 0.247 $cm^2 \cdot kV^{-1} \cdot s^{-1}$.

employed in the measurement of q was operating close to its lower limit. However, since q is fixed for all the data in Table 1, the ambiguity in q affects the slope of the regression line, but not its y intercept. Furthermore, since $FWHM_Z$ is relative to the size, the ambiguities in q and Q have no effect on the inferred values of either $FWHM_{Z\infty}$ or its standard deviation. Numerous repetitions of these measurements confirm the soundness of an intrinsic mobility width of 1.65 % or less for the 200 nm particles. Using Millikan's relation between mobility and size (Friedlander, 1977) at 200 nm, the corresponding $FWHM_d$ in diameter is 1.09 %. We are not aware of any prior report of such a narrow size distribution for suspensions of polymeric spheres in any size range, especially not at submicrometer sizes. For example, the commercial particles previously referred to at a similar mean diameter (≈200 nm) have $FWHM_d = 4$ %, almost four times wider that what was found here.

4. Results for 100 nm particles

The nominal 100 nm particles were in this case diluted 5-fold in deionized water. They were analyzed with the two DMAs already described: the Perez-MT-DMA used to study the 200 nm particles, and the Perez-LT-DMA (Perez-Lorenzo & Fernandez de la Mora, 2021) used to calibrate the Perez-MT-DMA. The LT-DMA covers nominally a size range up to 60 nm and is not ideal for analyzing particles as large as 200 nm at high resolution, yet it is well suited to investigate 100 nm particles. Fig. 6a shows the mobility distributions obtained with the previously calibrated LT-DMA, which give a peak at $Z = (0.2510 \pm 0.0006)$ $cm^2 \cdot kV^{-1} \cdot s^{-1}$ (mean mobility diameter $d = (103.8 \pm 0.2)$ nm). Again, the statistical uncertainty attached to these measurements is considerably smaller than the ±2 % uncertainty associated with the ambiguity in our measurement of the flow rate Q, which also propagates into the same relative uncertainty for the DMA calibration constants. The figure shows data taken at $Q = 24$ L/min ($z = 3$), 32.3 L/min ($z = 4$), and 40.7 L/min ($z = 5$), all in duplicate.

Fig. 6b shows the mobility spectra obtained with the MT-DMA. Their characteristics are collected in Table 2, obtained by fitting the data to two Gaussian curves, which yield an excellent fit to the main peak and the tail evidently present to its left. The mean mobility for the main mode in these seven spectra is (0.246 ± 0.003) $cm^2 \cdot kV^{-1} \cdot s^{-1}$, corresponding to a mean diameter of (105.1 ± 0.7) nm. The two lower spectra are clearly displaced to smaller mobilities, and may perhaps be the result of the conversion of the main peak into its satellite. This double peak structure suggests that the main, most mobile peak is contaminated by a less mobile peak. Both of these peaks are considerably wider than in the 200 nm particle distributions and are not well resolved from each other. In contrast, Fig. 6a shows a single relatively symmetric peak, uncontaminated by the low mobility feature seen in Fig. 6b.

The intrinsic variability in mean mobility seen in Fig. 6b and Table 2 is confirmed in Fig. 7 through various subsequent measurements using the LT-DMA and a new positive ES capillary. The primary measured quantity Z_1 is converted in Fig. 7 into particle diameter via Millikan's law (Friedlander, 1977). The broadest two duplicated curves shown were taken for the singly charged particles at a relatively small $Q = 8.15$ L/min. They are exceptional in resolving a bimodal distribution comprising a small-diameter mode at about 100 nm, and a larger mode at about 104 nm. The same bimodal structure shown at $Q = 8.15$ L/min in Fig. 7 was seen in several other higher charge states under the same spraying conditions. This lowest Q spectrum is also exceptional in showing a third mode at about 111.5 nm. All other spectra included in Fig. 7 under varying spraying conditions gave a single narrower mode at a mean diameter intermediate between 100 nm and 104 nm. Assuming that this size variability is due to different levels of crust of involatile solutes attached to the PSL spheres in the gas phase, it would seem that the smallest size obtained (≈100 nm) is the one closest to the true size of the spheres in the original suspension. The presence of two or three modes in these experiments suggests that the electrospray included drops of two or three different sizes, one unusually small and another unusually large. It is accordingly apparent that our current electrospraying technique is inadequate to produce a precise gas phase size standard with this 100 nm suspension. The considerably smaller size variability found with the 200 nm spheres may be the result of the smaller concentration of involatile solutes in that suspension.

In spite of the observed variability in mean size of the 100 nm spheres and their distribution width being substantially larger than in the 200 nm particles, these measured widths are still of interest. Table 2 reports the relative $FWHM_Z$ obtained by ignoring the tails on the left of the distributions. $FWHM_Z$ is in all cases close to 5 % (≈6 % using the full distribution). This corresponds to $FWHM_d = 3$ % in diameter. In spite of the possible magnification of the standard deviation of these distributions due to our imperfect electrospraying technique, they are nevertheless rather narrow for 100 nm particles ($FWHM_d = 5.2$ % for comparable 100 nm commercial reference particles).

5. Conclusions

* Our most interesting finding has been the exceptionally narrow size distribution of the 200 nm particles investigated. Previous results had already indicated this feature, but the present study with a DMA of high resolution provides an independent bound to the width of the size distribution, $FWHM_d < (1.09 \pm 0.05)$ % or $\sigma_d < (0.46 \pm 0.02)$ %.
* Our work also highlights the inability of the electrospraying technique to entirely avoid contamination of the aerosolized spheres from solutes in the suspension. Our best sprays for the 200 nm spheres appear to yield a clean small-diameter side for the size distribution (Fig. 4), but some tailing for the large-diameter side. The situation is considerably worse for the 100 nm particles.
* A substantial effort has been devoted to determine the origin of the secondary peaks associated with our electrosprays of the 200 nm particle suspensions. We find that comparable bimodal distributions arise in the original suspension as in derived suspensions containing no involatile solutes, both with and without addition of volatile electrolytes. These results leave us without a clue on how to eliminate the larger particle mode.

Table 2
Characteristics of the main peak for the 100 nm suspensions in Fig. 6b.

Q/z (L/min)	z	V_{DMA} (kV)	$FWHM_Z^{-1}$	Z_1 ($cm^2 \cdot kV^{-1} \cdot s^{-1}$)
35.0	1	8.162	19.5	0.250
35.0	1	8.168	19.5	0.249
35.1	2	8.277	20.0	0.247
35.1	2	8.258	20.0	0.247
35.1	3	8.264	19.4	0.247
35.1	3	8.456	19.3	0.242
35.1	3	8.456	19.3	0.242

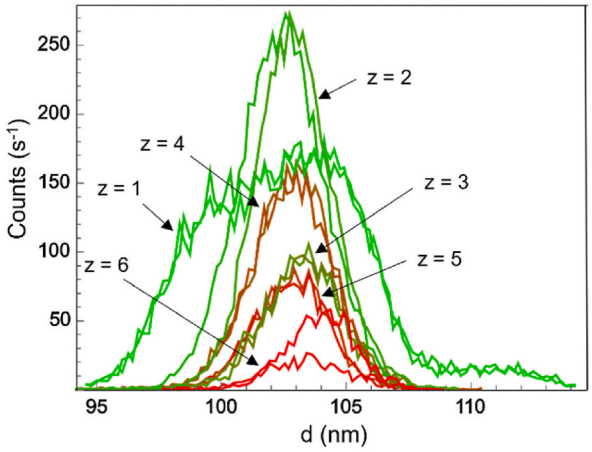

Fig. 7. Variability of the measured size distribution of 100 nm PSL particles under various charge states and sheath gas flow rates Q.

* While we believe our determination of the relative width of the size distribution of the particles investigated is accurate, a cautionary remark is in order. The widths measured are for the electrosprayed particles in the gas phase, with their attached crust of involatile solutes, rather than the original particles in the suspension. We trust the width found for the 200 nm particles when ignoring their low mobility tails is close to the true value for the suspension. However, that found for the 100 nm particles must be interpreted as an upper bound to the real value.

Declaration of competing interest

The authors declare that they have no known competing financial interests or personal relationships that could have appeared to influence the work reported in this paper.

Data availability

Data will be made available on request.

Acknowledgment

We are grateful to Drs. Luis Javier Perez-Lorenzo, Michel Attoui and Greg Lewis of Aerosol Dynamics for their many contributions to the experimental apparatus used for the mobility measurements. We thank the NanoEngineering Corporation for the gift of key components of an electrospray source, taken from their developing commercial version of our experimental system. We thank Dr. George W. Mulholland for several illuminating discussions relating to mobility measurement of other PSL particles. This work has been funded in part by AFOSR grant FA9550-22-1-0097.

Appendix A. Supplementary data

Supplementary data to this article can be found online at https://doi.org/10.1016/j.jaerosci.2023.106158.

References

Fernández-García, J., & Fernández de la Mora, J. (2013). Measuring the effect of ion-induced drift-gas polarization on the electrical mobilities of multiply-charged ionic liquid nanodrops in air. *Journal of the American Society for Mass Spectrometry, 24*, 1872–1889.

Fernández-García, J., & Fernández de la Mora, J. (2014). Electrical mobilities of multiply-charged ionic-liquid nanodrops in air and carbon dioxide over a wide temperature range: Influence of ion–induced dipole interactions. *Physical Chemistry Chemical Physics, 16*(38), 20500–20513.

Fernandez de la Mora, J. (2022). A singularly narrow 29 nm aerosol size standard based on the FX174 bacteriophage. *Journal of Aerosol Science, 161*, Article 105949.

Fernandez de la Mora, J., & Barrios, C. (2017). A Bipolar electrospray source of singly charged salt clusters of precisely controlled composition. *Aerosol Science and Technology, 51*(6), 778–786, 2017.

Fernández de la Mora, J., & Loscertales, I. G. (1994). The current emitted by highly conducting Taylor cones. *Journal of Fluid Mechanics, 260*, 155–184, 1994.

Fernandez de la Mora, J., Perez-Lorenzo, L. J., & Wick, D. (2020). Singularly narrow viral size and mobility standards from the 38.3 nm chronic bee paralysis virus and its 17.5 nm satellite. *Analytical Chemistry, 92*(20), 13896–13903.

Friedlander, S. K. (1977). *Smoke dust and haze*. Wiley. Equations (1.1), (2.16-2.17), (2.23.

JCGM. (2008). *Joint committee for guides in metrology evaluation of measurement data - guide to the expression of uncertainty in measurement (GUM)* (Vol. 100), 2008 https://www.bipm.org/documents/20126/2071204/JCGM_100_2008_E.pdf.

Kaufman, S. L., Skogen, J. W., Dorman, F. D., Zarrin, F., & Lewis, K. C. (1996). Macromolecule analysis based on electrophoretic mobility in air: Globular proteins. *Analytical Chemistry, 68*, 1895–1904.

Kim, J. H., Mulholland, G. W., Kukuck, S. R., & Pui, D. Y. H. (2005). Slip correction measurements of certified PSL nanoparticles using a nanometer differential mobility analyzer (Nano-DMA) for knudsen number from 0.5 to 83. *J. Res. Natl. Inst. Stand. Technol., 110*, 31–54.

Kinney, P. D., Pui, D. Y. H., Mulholland, G. W., & Bryner, N. P. (1991). Use of the electrostatic classification method to size 0.1 μm SRM particles - a feasibility study. *J. Res. Natl. Inst. Stand. Technol., 96*(2), 147–176.

Knutson, E., & Whitby, K. (1975). Aerosol classification by electric mobility: Apparatus, theory and application. *Aerosol Science, 6*, 443–451.

Mulholland, G. W., & Bauer, B. J. (2000). Nanometer calibration particles: What is available and what is needed? *Journal of Nanoparticle Research, 2*(1), 5–15.

Mulholland, G. W., Donnelly, M. K., Hagwood, C. R., Kukuck, S. R., Hackley, V. A., & Pui, D. Y. H. (2006). Measurement of 100 nm and 60 nm particle standards by differential mobility analysis. *J. Res. Natl. Inst. Stand. Technol., 111*(4), 257–312.

Myojo, T., Ehara, K., Koyama, H., & Okuyama, K. (2004). Size measurement of polystyrene latex particles larger than 1 micrometer using a long differential mobility analyzer. *Aerosol Science & Technology, 38*, 1178–1184.

Perez-Lorenzo, L. J., & Fernandez de la Mora, J. (2021). Exceeding a resolving power of 50 for virus size determination by Differential Mobility Analysis. *Journal of Aerosol Science, 151*, Article 105658.

Perez-Lorenzo, L. J., Khanna, V., Meena, T., & Fernandez de la Mora, J. (2020). A high resolution DMA covering the 1-67 nm size range. *Aerosol Science & Technology, 54*(1), 128–142.

Rayleigh, L. (1945). *The theory of sound* (Vol. 2, pp. 371–375). Dover Publications.

Tammet, H. (1995). Size and mobility of nanometer particles, clusters and ions. *Journal of Aerosol Science, 26*(3), 459–475.